

Chapter 1

Importance of Topology in Materials Science



Sanju Gupta and Avadh Saxena

Abstract We underscore the substantial need for understanding a wide range of multifunctional materials through the notions of topology-geometry interrelationships such as genus, Euler characteristic and network connectivity. After introducing the basic concepts of topology we first illustrate these notions on nanocarbon allotropes as a case study. Next, we consider the growing class of emergent topological materials that encompass both real-space and k-space topological materials including Dirac materials, topological insulators, Weyl semimetals as well as soft and polymeric matter, supramacromolecular assemblies and biophotonic materials. Finally, we emphasize and evaluate metrics to quantify topology in order to study and classify materials properties relevant for wide ranging modern and future technologies.

1.1 Introduction

The recent blooming of topological notions in condensed matter physics, synthetic materials chemistry, supramacromolecular chemistry, materials science and biophysics has given impetus to the development of new and the revision of many old concepts in the physical world [1, 2]. These sub-disciplines are being greatly benefitted by invoking topological concepts to understand novel, complex and emergent states of matter such as quantum Hall systems, topological insulators, Dirac materials and Weyl semimetals, to name just a few of these new classes of materials. The 2016 Nobel Prizes in Physics and Chemistry are a direct testament to this observation [1]. If the mainstream materials science can tap into the full power of

S. Gupta (✉)

Department of Physics and Astronomy, Western Kentucky University, Bowling Green, KY 42101, USA

e-mail: sanju.gupta@wku.edu

A. Saxena (✉)

Theoretical Division, Los Alamos National Laboratory, Los Alamos, NM 87545, USA

e-mail: avadh@lanl.gov

© Springer International Publishing AG, part of Springer Nature 2018

S. Gupta and A. Saxena (eds.), *The Role of Topology in Materials*,

Springer Series in Solid-State Sciences 189,

https://doi.org/10.1007/978-3-319-76596-9_1

topology, that would certainly open avenues for novel materials synthesis, property characterization as well as applications [2, 3].

Our aim in this chapter is to answer the key question: why is topology important for understanding materials? Topology refers to the fact that certain materials properties remain invariant under continuous deformation such as stretching, bending or twisting (but without cutting or puncturing at any place in the material systems). It also means that nearby points remain neighbors during deformation. In this sense a sphere and ellipsoid are topologically equivalent; so are a cone and disk [2].

First and foremost, we can classify the global topology of a material in terms of its characteristic genus (or handlebars or holes), number of open boundaries and local connectivity. Different topological phases of matter can be distinguished by a topological invariant (usually an integer such as the genus, Chern number, winding number, etc.) [1]. While a carbon nanoring and NbSe₃ Möbius strip represent real-space topological materials, recent interest in Dirac materials and topological insulators refers to topology in the k - or momentum space usually in terms of the electronic band structure. Quantum oscillations such as the de Haas-van Alphen (dHvA) and Shubnikov-de Haas (SdH) oscillations are a direct consequence of the topology of the Fermi surface of a crystal in a magnetic field. Based on these and many other illustrative examples mentioned below, we aim to show that the intersection of topology and materials science is both physically insightful and aesthetically appealing.

1.2 Essentials of Topology

1.2.1 Genus and Euler Characteristics

First, we introduce the basics of topology. Global topology of a material is described by a parameter called genus (g), which is an integer characterizing number of holes [2]. For instance it is zero for a sphere but equal to one for a torus. The genus is related to another parameter (of a surface) called the Euler characteristic, defined by $\chi = 2(1 - g)$. For objects with boundaries or edges it can be expressed as $\chi = V - E + F$, where V , E and F represent the number of vertices, edges and faces of a polyhedron on the object. The integral over the surface of a material's Gaussian curvature K gives 2π times the Euler characteristic (the Gauss-Bonnet theorem), connecting geometry with topology.

1.2.2 Network Topology

In the context of supramacromolecular architectures metal-organic frameworks (MOF) and geometric hierarchies inherent to many soft- and biomaterials (e.g. intra-

cellular structures such as endoplasmic reticulum), topology arises in a different guise, namely, network topology [2]. Here one focuses on local connectivity at a given node in the network, i.e. the number of links emanating from a particular node in the network. Two networks can have identical topology even though their physical interconnections or links, distances between the nodes and other attributes (e.g. transport of some quantity through the links) may differ. In biology network topology may refer to the network of biological interactions, for instance the metabolic network. Topologies commonly observed in biological networks include ring network, bus network and star network. As examples of the important role of network topology in materials, note that sound propagation in granular materials and mechanical properties of, e.g. siloxane, elastomers crucially depend on their network topology.

1.2.3 Geometry-Topology Interrelationship

As shown in Fig. 1.1 a cup can be continuously deformed into a sphere, thus they have $g = 0$ and $\chi = 2$. A cup with a handle is equivalent to a donut ($g = 1$, $\chi = 0$), but with two handles it is equivalent to a double-donut (or Swedish pretzel, $g = 2$, $\chi = -2$). In the same vein, a cup with three handles can be continuously deformed into a triple-donut (or German pretzel, $g = 3$, $\chi = -4$). A red blood corpuscle (RBC), a biological vesicle with one hole, two holes and three holes, respectively, represent $g = 0, 1, 2$ and 3 or $\chi = 2, 0, -2$ and -4 objects. Since topology is essentially elastic geometry, many different geometries may correspond to the same topology, i.e. same g and χ . Likewise, a variety of geometrically different networks may belong to the same topology, that is, a network with given geometry can be continuously deformed to obtain a network of different geometry.

1.3 Topological Taxonomy of Functional Materials

1.3.1 Nanocarbons

Carbon offers a rich variety of forms depending upon the covalent bonded hybridization, i.e. sp^3 -, sp^2 - and sp -bonded carbons. They exist in at least two natural allotropes (diamond, graphite) and various man-made or synthetic nanoscale forms (fullerenes, nanodiamond, carbon nanotubes and graphene). For the past few decades, there is an overwhelming interest in the family of nanocarbons due to their discernible structural characteristics at molecular scale and extraordinary physical (optical, mechanical, electronic) and chemical (electrochemical, biological etc.) properties attributed to their unique low-dimensional atomic scale lattice bonding structure. Therefore, they serve as functional building blocks for innovative nanotechnology such as in ultra-sensitive low-energy consumption electronics and mechanical devices, advanced cat-


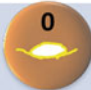

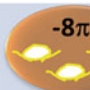




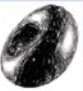

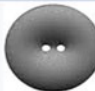

Object	Ball	Bagel	Swedish Pretzel	German Pretzel
Bagel, Pretzels				
Cup				
(g, χ)	(0, 2)	(1, 0)	(2, -2)	(3, -4)
Biological vesicles				

Fig. 1.1 Illustrations of topological objects with different genus, adapted in part from Haldane's 2016 Nobel lecture (top two rows) and [1], last row

alyst supports, sensitive biosensors, and microelectromechanical (micro-actuators) and electrochemical energy conversion and storage (e.g. fuel cell, batteries and supercapacitors) devices. Nanoscale carbons serve as a posterchild for the contexts where the interplay of geometry and topology is promising for basic and applied sciences. Nanocarbon allotropes exhibit numerous topologies with a variety of geometries ranging from planar (monolayer and multilayer graphene) to closed cage-like (e.g. fullerenes, hypo- and hyperfullerenes), open-ended (e.g. single-, double-, oligo- and multi-walled nanotubes), nano rings/nanotori, nanohorns, nanocones and peapods. All these distinct allotropes of nanocarbon serve as a fertile playing field for expounding the nontrivial notions of global topological attributes (see Table 1.1) [3–5]. Table 1.1 summarizes the global topology metrics of nanocarbons in terms of genus, g and Euler's characteristic, χ . Briefly, we indicate that nanocones, nanodisks and nanotubes closed at one end are topologically equivalent to a planar graphene sheet ($g = 0$). Fullerenes (C_{60}), hypofullerenes ($C_{36, 50, \dots}$), hyperfullerenes ($C_{70, 84, 90, \dots}$) and capped nanotubes have the topology of a sphere ($g = 0$). Due to boundaries captured by χ , open ended nanotubes have a different topology ($g = 1, \chi = 0$) than those of closed nanotubes ($g = 0, \chi = 2$). Nanotori and nanorings forms of nanocarbon are topologically equivalent to a torus ($g = 1, \chi = 0$). Furthermore, multi-walled carbon nanotubes, nano-onions and peapods (fullerenes nestled in single-walled carbon nanotubes like a beaded necklace) have complex topologies due to nested spherical and cylindrical geometries. Among the negative Gaussian curvature ($K < 0$) periodic carbons, Schwarzites have a complex topology with $g = 3, \chi = -8$ per unit cell. Similarly, a helicoid-shaped narrow graphene nanoribbon would have $g = 0, \chi = 2$ [5].

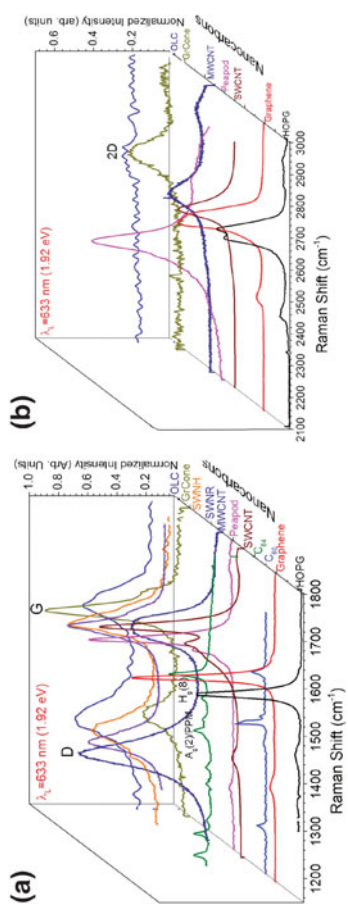
Table 1.1 Topology of nanocarbon allotropes

Geometry	Topological characteristics	
	g (Genus)	χ (Euler)
Positive Gaussian curvature		
Mono-, few- and multi-layer graphene (HOPG and Kish Graphite)	0	2
Fullerenes and hypo-/hyperfullerenes	0	2
Single-walled carbon nanotube (SWCNT); open (closed)	1 (0)	0 (2)
Nanoring/nanohoop/nanotori	1	0
Nanohorn/nanocone	0	2
Double-walled (DWCNT), oligo-walled (OWCNT) and multi-walled carbon nanotube (MWCNTs)	Complex geometries	
Peapod		
Onion-like carbon (OLC)		
Negative Gaussian curvature	g (Genus) unit cell	χ (Euler)
Negatively curved carbons/Schwarzites (3D)	3	-8
Graphene nanoribbons (GNR)/helicoidal (2D); infinite (finite)	0 (0)	2 (1)

Our goal here is to relate measurable physical properties deduced from resonance Raman spectra of various nanoscale carbons to topological as well as geometric metrology characteristics. Spontaneous Raman spectroscopy (RS) has emerged inarguably as a powerful non-invasive analytical tool for structural characterization of carbon-based materials revealing both collective atomic/molecular motions and localized lattice vibrations (phonons) [3] besides defects (point or extended defects, stacking disorder, doping) and finite size of crystallites. The primary reason for this advantage is the strong Raman scattering response to the π states due to resonance enhancement, its simplicity for high-symmetry nanotubes and fullerenes, its easy access and noninvasive nature. Figure 1.2 shows micro-Raman spectra for various nanocarbons measured using excitation wavelength of 633 nm (or energy $E_L = 1.92$ eV) in backscattered configuration. Since all of these materials are sp^2 C derivatives, it is instructive to compare the Raman spectral features with planar highly ordered pyrolytic graphite (HOPG) or multilayer graphene (MLG) and monolayer graphene as they are two-dimensional building blocks for sp^2 C allotropes of every other dimensionality. Prominent bands of interest in first- and second-order Raman spectra are D, G and 2D bands occurring at ~ 1344 cm^{-1} , ~ 1585 cm^{-1}

and $\sim 2670\text{ cm}^{-1}$, respectively. The G band is associated with the tangential C-C stretch or the tangential displacement band having E_{2g} symmetry. For SWCNT, the G band decomposes into main peaks (G^+ at 1562 cm^{-1} and G at 1593 cm^{-1}) primarily due to the splitting of interlayer stretching mode attributed to curvature-induced re-hybridization of $\sigma^*-\pi^*$ states which yields larger elastic constants and therefore better mechanical properties. The D band is a disorder-activated band with A_{1g} symmetry arising from various sources including in-plane substitutional heteroatoms, vacancies, grain boundaries, quantum confinement due to size effects, stacking disorder and other point and extended defects. Therefore, D band intensity in principle is proportional to the phonon density of states analogous to electronic density of states, applicable to all sp^2 C-based materials. It is worthwhile to note the near absence of D band in monolayer (and multilayer) graphene and HOPG indicative of presence of marginal defect number density. The stable sp^2 C spherical cage structures—fullerenes (C_{60})—are somewhat lower in yield and the effect of curvature and geometry is displayed in Raman spectral features for spheroids compared with HOPG and MLG. There are fewer lines for C_{60} (I_h symmetry) as compared to C_{84} (D_{2d} symmetry) possibly due to deviation from spherical geometry (oblate or prolate). While it is challenging to analyze complicated Raman spectra due to fullerenes, the downshift of $A_g(2)$ (pentagonal pinch mode; $\sim 1470\text{ cm}^{-1}$) and $H_g(8)$ band at $\sim 1575\text{ cm}^{-1}$ is apparent. Figure 1.2 also shows Raman spectral features due to SWNR, SWNH and nanocone displaying similar phonon spectra to sp^2 C material systems, *albeit* they have some quantitative differences discussed below. It is imperative to mention that for low-dimensional carbons (nanocarbons), the 2D band (a second-order D band) is symmetry allowed by momentum conservation, therefore the overtone Raman feature is relatively sharp and comparable to G band intensity in contrast to disorder-activated D band and it becomes an intrinsic feature for sp^2 C materials (Fig. 1.2b).

The prominent Raman bands for representative nanocarbon materials are quantitatively analyzed in terms of position of D, G and 2D bands as possible topological metrics due to their sensitivity toward structural modification and mechanical deformation as well as charge transfer doping thus capturing “weaker” or “group” trends. Figure 1.3 shows the variation of G band position by itself (panel a) and with 2D band (panel b) providing subtle information on curvature induced shifts and the nature of intrinsic point defects (charged or residual). For instance, G band is marginally upshifted in SWCNT as compared with SWNR leading to microscopic compressive stress attributed to smaller nanotube curvature that is invoked. The G band for nanocone tip and SWNH shifts to higher value as compared to HOPG; this occurs due to curved cone surface and phonon confinement attributed to smaller crystallite sp^2 C domains. While the presence of G band is a direct indication of sp^2 C network, the shift (either decrease or increase) is a measure of (a) different sp^2 -bonded C configurations; (b) curvature-induced re-hybridization and mixed hybridized character $sp^{2+\delta}$; (c) compressive or tensile microscopic stress/strain; and finally, (d) phonon confinement (localization of vibrational states) and (e) electronic character (n- or p-type). The tensile strain in graphene planes induces curvature by the introduction of pentagons in the hexagonal network governed by Euler’s theorem.



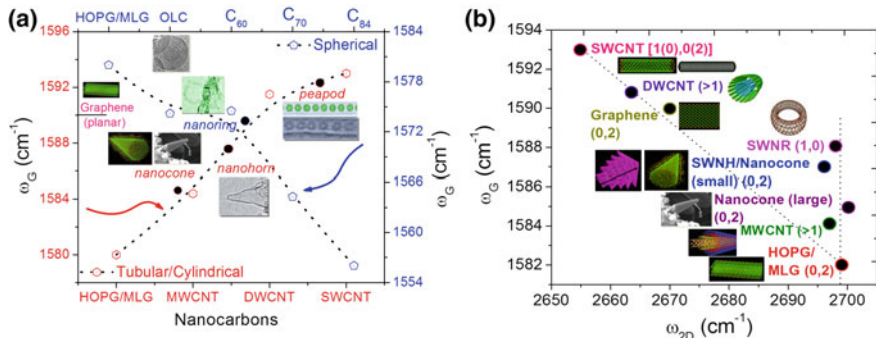


Fig. 1.3 Variation of the position of **a** G band and **b** 2D band with G band from Raman spectra for various nanocarbons along with HOPG and MLG. The values of (g, χ) are also shown in parentheses

While the Raman bands for the nanocone and nanohorn appear at almost similar positions, the nanoring lies in the category of a different geometry. A quantitative understanding of Raman lineshape and band position shifts occurring due to geometry and topology therefore require a detailed accounting for the changes in both phonon and electronic density of states and concurrent electron-phonon (lattice) interactions suggested by theoretical studies for nanotori, nanocones and nanohorns [6, 7]. We have made an attempt to determine the nature of the defects by plotting the 2D band position with the G band position (see Fig. 1.3b) [8]. It is safer to say that the defects are mainly *p*-/*n*-type (i.e. the G band increases and the 2D band decreases), which is quite encouraging. Furthermore, the quantitative findings obtained from Raman spectra are also in agreement with tight-binding calculations for the nanotubes [8]. This knowledge provides a powerful geometric (and possibly topological) metrology machinery to understand novel nanocarbons and points to an unprecedented emergent paradigm in materials science i.e. global topology (and curvature) \rightarrow process \rightarrow property \rightarrow function \rightarrow performance relationships in contrast to traditional microstructure \rightarrow property \rightarrow function correlations.

1.3.2 Soft and Polymeric Materials

Analogous to nanocarbons, hard-, soft- and polymeric (liquid crystal supermolecules and supramolecular chemistry) materials exist in a variety of complex topological phases and forms, summarized in Table 1.2. Some examples include semiconducting oxide and BN nanotubes, nanotori, helical gold nanotubes, mesoporous silica networks, Möbius conjugated organic materials, di-block and tri-block copolymers as well as smectic and nematic liquid crystals [2]. Also, foams have interesting network topology which can change its configuration at a local level, wherein the interface between two bubbles shrinks to zero length and subsequently expands to a finite

Table 1.2 Topology of soft-, polymeric, biological matter and supramolecular assemblies

Geometry	Topological characteristics		Suggested metrology
	g (Genus)	χ (Euler)	
Soap bubbles and foam	Network topology		Optical imaging
Liquid crystals (double and quadri-dislocations and disclinations; discotic, nematic with Schlieren texture)	Complex topology		Non-linear optical fluorescence microscopy, laser lithography
Di- and tri-block co-polymers (lamellar and tubular)	Complex topology		Small-angle x-ray and neutron scattering (SAXS/SANS)
Bio-membranes (lamellar and spherical)	0	2	Optical fluorescence microscopy and SAXS/SANS
Biological vesicles (w/ and w/o holes)	0/1, 1, 2	2/0, 0, -2	Optical fluorescence imaging
Zeolites (micro-/mesoporous, metallo-organic frameworks [MOFs])	3	-8	HRTEM, SAXS/SANS, x-ray and neutron tomography
Supramolecular assemblies	1	0	Optical fluorescence imaging and SAXS/SANS

length in another direction, thus resulting in a local topology change. For studying two- and three-dimensional microscopic structure evolution with regard to crystal grain growth and topological optimization of microstructure besides multicellular structures such as bubbles, foams, and biological tissues, network topology serves as an efficient tool [9].

As for polymeric liquid crystals which show complex topology—they are hard in that they have many interesting symmetries thus exhibit anisotropic elastic behavior, while their liquid properties enable a soft behavior such that these symmetries are disrupted by defect structures and their elasticity is dominated by fluctuations away from an ideal state. Analogous to all broken symmetry materials, liquid crystals admit topological defects, which are regions forced to be discontinuous by their topological behavior. Such defects are stable in the sense that they cannot be removed by local perturbation, rather they must either be moved out to the boundary of the sample or merged into other topological defects. Of utmost importance is the study of these topological defects, which are readily visualized. Since the behavior of materials is often dictated not by bulk properties, but by its defects, akin to the strength of a chain being determined by its weakest link. Historically, topological defects in ordered media were studied using the theory of homotopy classes in which homotopy

groups of the order parameter space are calculated [10–13]. These ideas begin with identifying defects with small measuring loops or spheres around them. Thus, the “charge” of the defect is the topological metric (i.e. genus) of the configuration in the sample on such a measuring circuit [14]. Given the development of three-dimensional imaging techniques [14] and extensive simulations [15, 16], one has a way of seeing more globally the topological defects and other interesting topological features in these samples. These sets include the defects but usually include other points forming lines or sheets connecting the defects together as well. In general, the homotopy group approach is not justified when applied to smectic liquid crystals or other crystalline systems. However, in these smectics there are two classes of defects, dislocation-type and disclination-type, which are akin to critical points in the sense of local maxima, minima or saddle points.

1.3.3 Minimal Periodic Surfaces

1.3.3.1 Supramacromolecular Assemblies

Micelles, colloids, micro-emulsions, biological vesicles, microtubules and supramolecular photochemistry in restricted space belong to this class of materials [2]. Additionally, processes in many bio-macromolecules including DNA and RNA structure and protein folding, involve network, braid and knot topologies [17]. A network has connected nodes and lines in various ways. Lattices are a special kind of network in which the lengths are the same in each periodically repeated structure, called a unit cell. Two networks (‘nets’) have different distances between nodes and other characteristics yet may have identical topologies. As a special case, a square lattice is topologically equivalent to an oblique lattice or a rectangular lattice but not to a triangular Kagome-like lattice. Protein-protein interaction networks (‘interactomes’), and mesoporous materials are examples in which correlations between the network structure and properties provide useful insights into design strategies.

Metal-Organic Framework, (MOFs, pronounced *moffs*), are compounds consisting of metal ions or clusters coordinated to organic ligands to form one-, two-, or three-dimensional structures (Fig. 1.4). They are a subclass of coordination polymers, with the special feature that they are mesoporous. The organic ligands included in them are sometimes referred to as “struts”, one example being 1,4-benzenedicarboxylic acid (BDC). More formally, a metal–organic framework is a coordination network with organic ligands containing potential voids. A coordination network is a coordination compound extending through repeating coordination entities in one dimension, but with cross-links between two or more individual chains, loops, spiro-links, or a coordination compound extending through repeating coordination entities in two or three dimensions; and finally, a coordination polymer is a coordination compound with repeating coordination entities extending in one, two, or three dimensions [18]. The study of MOFs has been developed from the study of zeolites, except for the use of preformed ligands. MOFs and zeolites are

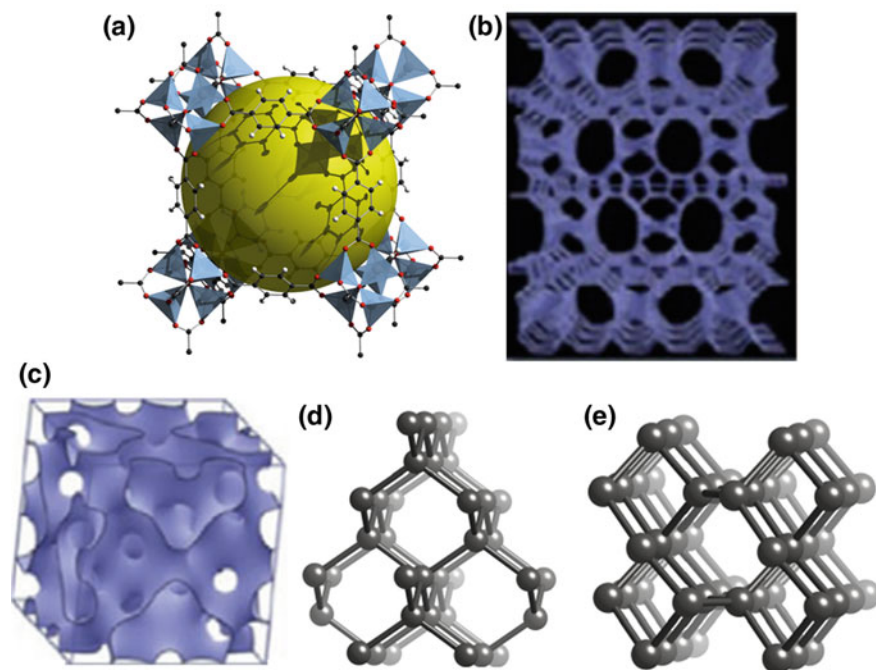


Fig. 1.4 Example of **a** MOF-5 and **b** zeolite catalyst. Corresponding **c** double gyroid and **d, e** network topologies with four-connected branching points (**dia**-net based on diamond structure) or vertices (chiral **qtz**-net based on quartz structure) [19]

produced almost exclusively by hydrothermal or solvothermal techniques, where crystals are slowly grown from a hot solution. In contrast, MOFs are constructed from bridging organic ligands that remain intact throughout the synthesis [19]. In some cases, the pores are stable during elimination of the guest molecules (often solvents) and could be used for the storage of gases such as hydrogen and carbon dioxide. Other possible applications of MOFs are in gas purification, gas separation, electro- and photocatalysis, as sensors, energy harvesters and supercapacitors [20].

1.3.3.2 Biophotonic Materials

The topology of mixed di- and triblock copolymers as well as single and double gyroids in butterfly wings, weevil chitin and bioinspired photonic bandgap crystalline materials, zeolites and other metallo-organic frameworks belongs to triply periodic minimal surfaces. Depending upon the relative concentration of the constituents, temperature and pressure, the topology of block copolymers and biomacromolecular systems can change from lamellar, globular, and tubular to gyroid and double gyroid structures [21–23]. The self- and directed-assembly of block copolymers result in

complex topologies (third row, Table 1.2) as a function of relative concentration of different types of polymer blocks and the interaction energy between different types of monomers. Interestingly, the gyroid is a triply periodic minimal surface where mean curvature $H = 0$ that belongs to the family of P (primitive) and D (diamond) Schwarz surfaces and it separates space into two identical labyrinths of passages discovered by Alan Schöen in 1970.

Biomembranes can be flat (lamellar) or curved depending on the structures they enclose (fourth row) [24] and they can also morph into a spherical or toroidal topology, in some cases with $g > 1$ (fifth row). As indicated, MOFs [25] also form periodic minimal surfaces and gyroid-like structures (sixth row). Finally, supramolecular assemblies may emerge with a variety of topologies, including spheroidal, periodic with $g = 1$, or even a gyroid-like structure [26]. It is thus highly desirable to probe and quantify the topological attributes of the examples portrayed in Table 1.2.

We reiterate that topology finds its multifaceted presence in a variety of biological materials, particularly in the context of biophotonics. Some interesting examples include polarized iridescence in jewel beetle, butterfly chitin, bird keratin [27] and gyroid-type photonic crystals in diamond weevil and wing scales [28].

1.4 Topological Phases in Condensed Matter

Topological materials: Materials in which topological aspects, usually involving boundary effects such as surface or edge effects, alter the electronic, transport, magnetic and various other properties are christened as topological materials [29]. In particular, topological superconductors, topological insulators, topological crystalline insulators, and some Dirac materials (e.g. Weyl semimetals and graphene) are important members of this class. To understand topological invariants and the properties of these materials, topological field theory has been developed recently [30]. Finally, we note that some of these materials can possibly support the so called non-abelian particles (or elementary excitations) called anyons, Majorana fermions being an example, which can enable the current pursuit of topological quantum computing through the braiding statistics of Majorana fermions. The latter paradigm is a viable approach for fault-tolerant quantum computation currently under consideration [31].

Topological defects: In general, certain material defects that interpolate between two different orientation states, e.g. domain walls and those resulting from certain material discontinuity, for instance disclinations and dislocations, constitute the broad class of topological defects. Monopole-like excitations and out-of-plane vector configurations, e.g. skyrmions and vortices, also belong to this class [2]. Clearly, such defects alter the macroscopic properties of materials, e.g. strength, electronic transport and magnetic response. Since the presence of topological defects affects materials properties in unusual ways; it is imperative that we are able to control experimentally the density and generation of these defects.

1.4.1 Real-Space Topological Materials

While most of the topological materials discussed below such as topological insulators and Weyl semimetals deal with topology in the momentum or k -space, e.g. the topology of the Fermi surface, synthesizing topological crystals in real space is both intriguing and important. In fact, a Möbius strip has been synthesized using a crystalline ribbon of NbSe_3 , which is a low-dimensional inorganic conductor exhibiting charge-density-waves (CDW). The width of such a strip is about one micron whereas the ring diameter is about 100 μm . Similarly, figure “eight” structures with a double twist, knot crystals and Hopf link materials have also been synthesized [32–34]. Interestingly, the various topological arrangements of NbSe_3 all show CDW phase transitions. Such topological variants can also be synthesized using TaSe_3 and TaS_3 .

Changes in topology with a twist singularity have been observed in soap-film Möbius strips [35]. In this process the linking number of the film’s Plateau border and the centerline is altered. Similarly, simulations based on a discrete, lattice based model have demonstrated the influence of a material’s stretchability on the equilibrium shape of a Möbius strip [36].

1.4.2 Dirac Materials

The (nonrelativistic) Schrodinger equation describes conventional metals, semiconductors and insulators, for which the electronic energy dispersion of low-lying excitations is quadratic: $E_S = p^2/2m^*$. Here p denotes the electron momentum and m^* the effective mass. In contrast, there is a growing family of materials with electronic band structure that exhibits linear dispersion (Fig. 1.5), called Dirac materials [37, 38]. One salient feature of these materials is that their valence and conduction bands touch at a few isolated points known as the Dirac points (and the associated band attributes are called the Dirac cones). These points remain unaltered under perturbations, or equivalently are *topologically protected*, as a consequence of certain symmetries. For graphene, it is the sublattice symmetry, for topological insulators it is the time-reversal symmetry [39, 40] whereas for topological crystalline insulators [41, 42] it is the mirror (or a related crystalline) symmetry. In the case of two-dimensional Dirac materials (that are described by the relativistic Dirac equation) the electronic energy dispersion is linear in momentum, $E_D = c \sigma \cdot p + mc^2 \sigma_z$. Here $\sigma = (\sigma_x, \sigma_y)$ are Pauli matrices and the Fermi velocity v_F replaces the speed of light in the material.

An important implication of the linear dispersion of Dirac materials is their enhanced sensitivity to applied magnetic field in two dimensions. Specifically, electronic energy level spacing is proportional to \sqrt{B} in massless Dirac materials in contrast to B in usual materials. The electronic Dirac spectrum in topological insulators, d-wave superconductors and graphene has been measured using angle resolved photoemission spectroscopy (ARPES) as well as scanning tunneling spectroscopy (STS) [37]. Beyond graphene, silicon and germanium monolayer structures named

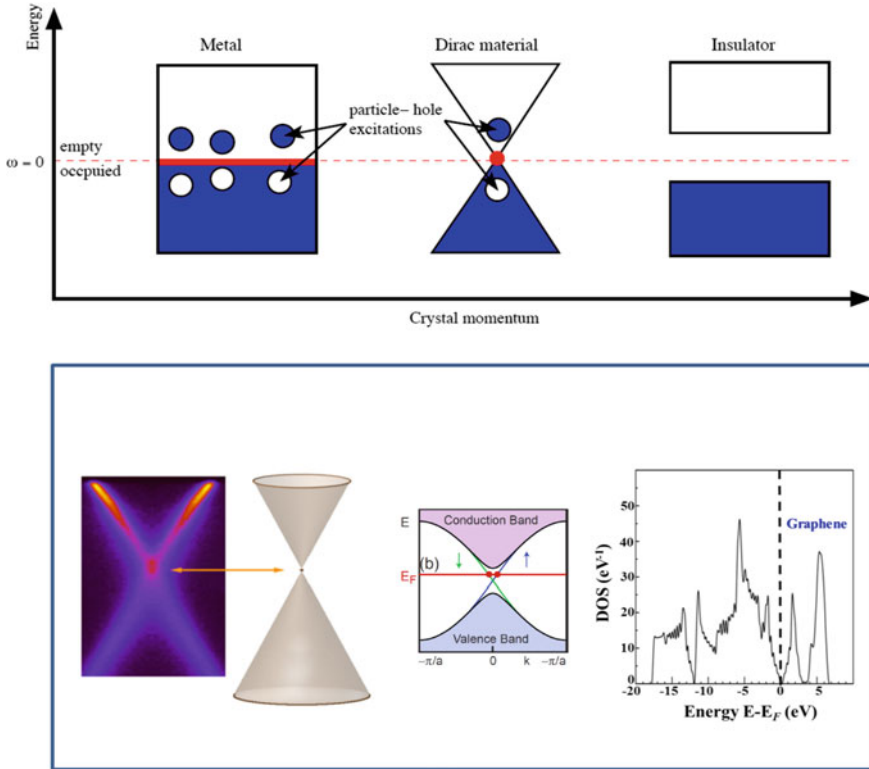


Fig. 1.5 (Upper panel) Schematic band diagrams for metals without a gap (left), Dirac materials exhibiting linear band dispersion as well as a Dirac cone (middle) and insulators with a band gap (right). (Lower panel) Angle-resolved photoemission spectroscopy (ARPES) results for graphene obtained at the Advanced Light Source at LBNL and the corresponding DFT calculations of density of states. Adapted in part from [37]

silicene [43], germanene [44], and sp^2 carbon allotropes called graphynes [45] also exhibit Dirac cones and thus belong to the growing family of two-dimensional Dirac materials. Related honeycomb monolayers of phosphorus and tin called phosphorene [46] and stanene [47], respectively, represent novel two-dimensional topological materials. Even a lead based monolayer called plumbene has been theoretically proposed.

Nodal line insulators and semimetals: In some topological semimetals, such as the strongly spin-orbit coupled compound PbTaSe_2 , valence and conduction band touch at one-dimensional Fermi lines known as nodal lines [48]. Unlike the (zero-dimensional) Weyl points, which are protected against perturbations that preserve translational symmetry, the protection of nodal lines requires additional crystal symmetries, e.g. mirror reflection. They have been studied using ARPES [48], and are also characterized by an integer topological invariant. Electronic structure calcula-

tions of these materials and relevant experiments are discussed in Chap. 6 in this book.

There are three kinds of spin half-integer particles (e.g. electrons) in nature called fermions that can occur in condensed matter and materials as well as in photonics: Majorana, Dirac and Weyl. For particles with mass and linear dispersion, graphene represents a prime example of Dirac particles. Materials comprising particles without mass but with linear dispersion are called Weyl materials or Weyl semi-metals, e.g. NbAs, NbP, TaAs and TaP [49, 50]. There has been an intense search for such materials in recent years. These materials can be viewed as three-dimensional analogs of graphene with broken time reversal and spatial inversion symmetry. Note that Weyl semimetals can be characterized by the experimental observation of Fermi arcs in ARPES [51]. Interestingly, they can also exhibit magnetic monopoles in the crystal momentum (or reciprocal) space. Particles that possess mass and are also their own antiparticles are termed Majorana fermions. There has been a great deal of experimental search for Majorana fermions [50]; it is anticipated that topological superconductors [52, 53] might possess them as quasi-particles. Beyond their fundamental significance, there is growing excitement about their role in topological quantum computing [31].

1.4.3 Topological Insulators and Topological Superconductors

Topological insulators (TI), which are metallic at the surface and insulating in the bulk, and related materials usually have a strong spin-orbit coupling [39, 40]. It is worth noting that until the discovery of quantum Hall effect (QHE) in 1980 it was believed that all fundamental laws of nature and phases could be understood in terms of symmetry (and geometry). However, QHE provided the first instance of a quantum state with no spontaneous broken symmetry. The behavior of QHE depends only on the system's topology and not its specific geometry thus opening up the frontier field of topological order.

The first two-dimensional TI was discovered in HgTe quantum wells [29]. This topological state is also known as the quantum spin Hall state. Band inversion is the main mechanism herein where the spin-orbit coupling inverts the usual ordering of conduction and valence band. Subsequently, three-dimensional topological insulators were discovered in materials such as Bi_2Se_3 , Bi_2Te_3 and Sb_2Te_3 . The band inversion in these materials occurs at the Brillouin zone center due to the spin-orbit coupling [29]. The topological surface state comprises a helical Dirac fermion in that the electron spin is perpendicular to its momentum; in other words it forms a left-handed helical texture in momentum space. No gap for the surface state can be introduced by a time reversal invariant perturbation.

Topological insulators can also exist *without* spin-orbit coupling in the presence of certain crystal point group symmetry. They are called topological crystalline insu-

lators (TCI). SnTe is a prime example of a topological crystalline insulator [41, 42]. Lattice periodicity is not a requirement and even quasicrystals can display TI behavior under appropriate conditions. Recently, a two-dimensional quasicrystal in the presence of a uniform magnetic field exhibited chiral edge states (in analogy with Chern insulators in periodic lattices). Such materials have been christened as topological Hofstadter insulators [54].

The proximity of a superconductor to the surface of a topological insulator can result in a topological superconductor [52, 53]. The latter is characterized by the presence of Majorana zero modes. In essence, topological superconductivity involves edge-mode superconductivity in topological insulators. Note that two-dimensional topological superconductivity in InAs/GaSb [53] and three-dimensional superconductivity in $\text{Cu}_x\text{Bi}_2\text{Se}_3$ [52] has been experimentally observed. Another example of such a material is Sr_2RuO_4 (possibly with chiral p-wave superconductivity). We emphasize that the Berry phase (in momentum space) plays a key role in TI and topological superconductors.

We can view TI in two ways: (i) as unusual band insulators with surface states (i.e. obtaining a 3D state from 2D), and (ii) as materials with a quantized magnetoelectric response (i.e. obtaining a 2D state from 3D). In essence, the notion of TI is a generalization of the idea of integer quantum hall effect (IQHE). In particular, a system of noninteracting lattice fermions with broken time-reversal symmetry can exhibit IQHE, which is characterized by a topological invariant called Chern number and is stable against disorder and interactions. Analogously, a system of noninteracting Bloch fermions with unbroken time-reversal symmetry corresponds to TI. Akin to fractional QHE there may well exist fractional TI [55].

1.4.4 Weyl Semimetals

Weyl semimetals refer to solid state crystals whose low energy excitations correspond to Weyl fermions [56–58]. The latter carry electrical charge even at room temperature. These materials are a topologically nontrivial phase of matter (Fig. 1.6). Historically, in 1929 Hermann Weyl showed the existence of a massless fermion as a solution of the Dirac equation, now known as the Weyl fermion. These materials are three-dimensional analogs of graphene in that Weyl semimetals show linear dispersion around certain nodes in the Brillouin zone called Weyl points, which always appear in pairs. They also exhibit Fermi arcs (Fig. 1.6), which are unclosed lines that start from one Weyl point and end at the other with opposite chirality (Figs. 1.7 and 1.8), in addition to chiral magnetotransport.

TaAs represents a typical example of a (type-I) Weyl semimetal (Fig. 1.7). Other related materials such as WTe_2 and MoTe_2 belong to what are known as type-II Weyl semimetals [59, 60]. For a material to be a Weyl semimetal it must break either the lattice inversion symmetry or the time-reversal symmetry. In the case when these two symmetries coexist, there may exist a pair of degenerate Weyl points resulting

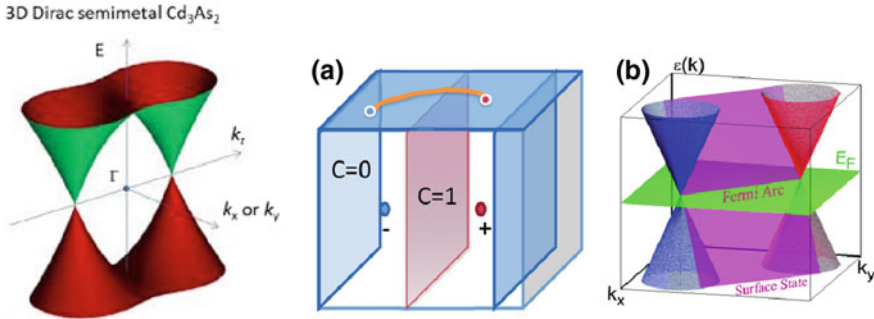


Fig. 1.6 A comparison of the double Dirac cone band structure for a Dirac semimetal (left panel) Cd_3As_2 and a Weyl semimetal TaAs (middle and right panels). For the Weyl semimetals (a) Fermi arcs connecting regions of different Chern numbers ($C = 0$ and $C = 1$) are depicted. (b) The corresponding Fermi level is also shown. Adapted in part from [56]

in what is known as a Dirac semimetal. Weyl fermions can be controlled by both the optical and electrical means (Fig. 1.9).

1.4.5 Other Topological Materials

In topological defects called magnetic monopoles (or magnetic charges) the effective magnetic field lines emanate from a point radially outward. Such defects have been likely observed in artificial spin ice (ASI) [61] as well as in current driven chiral magnets where skyrmion tubes merge or separate at an isolated number of points [62]. ASI is an assembly of nanomagnets in a particular lattice whereas skyrmion is a spin texture in which the spin orientation goes from 0 to π . Equivalently, the spin texture covers the unit sphere once. One could think of ASI as a *magnetolyte* in analogy with charges in an electrolyte. In these materials one expects a monopole-antimonopole pair to exist, which is connected by the so called Dirac string. There is a flux in the interior of a Dirac string which renders the presence of monopoles consistent with the requirements of Maxwell's equations. Both skyrmions and ASI are discussed in detail in Chaps. 4 and 5 in this book.

Penta-Graphene: Based on total energy calculations a new two-dimensional metastable carbon allotrope, composed entirely of pentagons (that resemble Cairo pentagonal tiling), has been proposed [63]. It was motivated by the recent proposal of T12-carbon phase, which can be chemically exfoliated to produce a single layer penta-graphene. This allotrope exhibits dynamical, thermal and mechanical stability in addition to a large band gap, ultrahigh mechanical strength and negative Poisson's ratio. It can withstand temperatures as large as 1,000 K. However, it still remains to be experimentally synthesized.

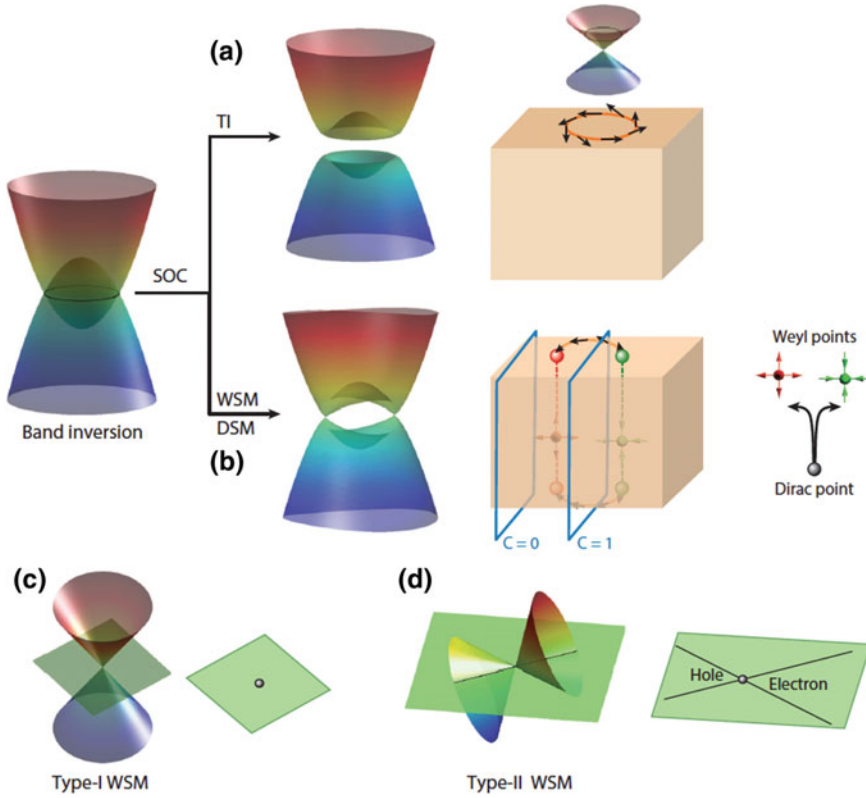


Fig. 1.7 Spin-orbit coupling (SOC) induced band inversion leading to the formation of topological insulators (TI), Dirac semimetals (DSM) and Weyl semimetals (WSM). **a** A full gap is opened in a TI resulting in metallic surface states. **b** In DSM and WSM bulk bands are gapped except at some isolated points with linear dispersion called Dirac points and Weyl points, respectively—they constitute a three-dimensional analog of graphene. **c** Type-I WSM in which the Fermi surface shrinks to zero at the Weyl points when these points are sufficiently close to the Fermi energy. **d** Type-II WSM: the Weyl points represent the touching points between the electron and hole pockets in the Fermi surface as a result of the strong tilting of the Weyl cone. Adapted from [59]

Rolled-up penta-graphene leads to penta-tubes: Carbon nanotubes solely comprising pentagons, which demonstrates the structural versatility of penta-graphene. Phonon calculations and *ab initio* molecular dynamics (AIMD) simulations demonstrate the dynamic and thermal stability of penta-tubes, respectively. Unlike carbon nanotubes, penta-tubes are semiconducting independent of their chirality [63]. Stacking of penta-graphene layers leads to a three-dimensional stable structure called AA-T12 carbon, which is also semiconducting and has properties quite different from T12-carbon. Both electronic structure and phonon dispersion have been calculated for this layered carbon allotrope. Analogous calculations also suggest a tetragonal phase of metallic three-dimensional boron-nitride [64].

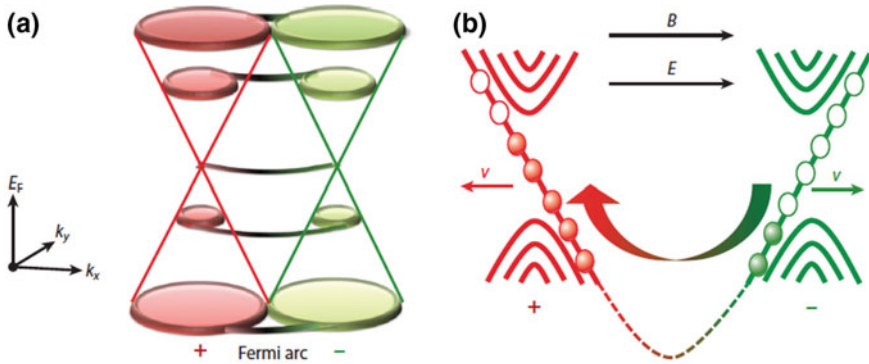


Fig. 1.8 Fermi arcs in the Fermi surface of the surface band structure of a Weyl semimetal. **a** A pair of Weyl cones (in two different colors) representing two different chiralities exist at nonzero Fermi energy or at zero Fermi energy. The Fermi arcs connect these two cones. **b** The chiral anomaly in these materials can be understood in terms of the zeroth Landau level in the quantum limit. E and B represent applied electric and magnetic fields. Adapted from [59]

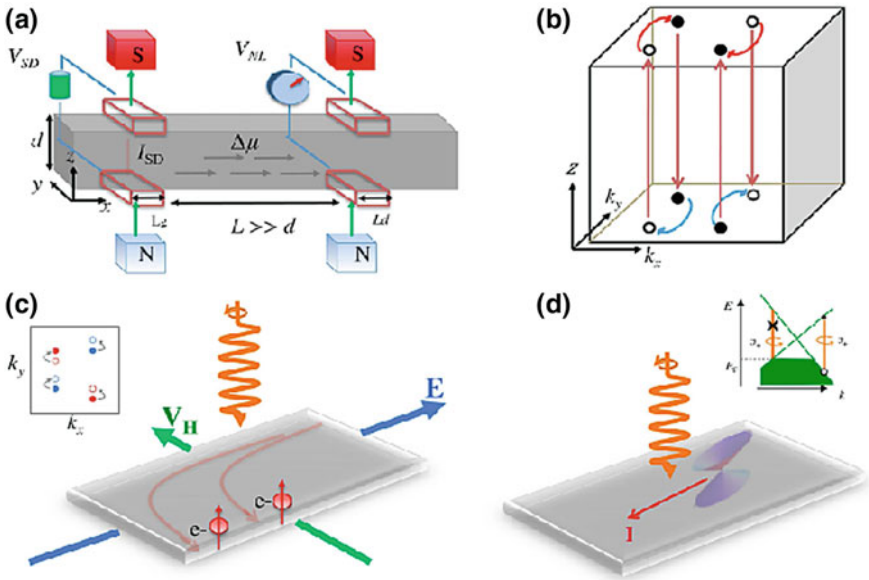


Fig. 1.9 Control of Weyl fermions by electrical and optical means. **a** A nonlocal electrical transport device utilizing axial current from the chiral anomaly. **b** Electrons exhibit unusual paths on the surface of a Weyl semimetal. **c** Time-reversal symmetry can be broken by shining an intense circularly polarized light. **d** A large photogalvanic current breaks inversion symmetry as well as any mirror symmetry in the presence of circularly polarized light. Adapted from [60]

Hepta-graphene: Based on density-functional-theory (DFT) calculations a dynamically stable, seven-membered carbon allotrope called hepta-graphene has been pre-

dicted [65]. It has a rectangular unit cell comprising ten carbon atoms and four hydrogen atoms. Its band structure is topologically equivalent to that of strongly distorted graphene, i.e. it has Dirac cones which are robust both under compressive and tensile strain. However, shear strain leads to a band gap, which is tunable. Note that systems without the hexagonal symmetry rarely exhibit Dirac cones; hepta-graphene is one such example.

Phagraphene: Another monolayer allotrope of carbon called phagraphene composed of pentagons, hexagons and heptagons has been proposed which also exhibits Dirac cones in a rectangular lattice and is robust against external uniaxial stress. However, similar to hepta-graphene a gap is opened in this material under shear stress [66]. A calculation of the phonon spectra demonstrates this allotrope is also dynamically stable (akin to hepta-graphene).

Phosphorene and its nanoribbons: Remarkably, the phosphorus analog of graphene called phosphorene has been synthesized, which is a promising candidate for thermoelectric applications [67]. Corresponding electronic, optical and transport properties have been studied for phosphorene as well as phosphorene nanoribbons including exciton effects. Interestingly, a related single-element based, monolayer material called borophene [68] has been found to exhibit Dirac cones in addition to two sublattices with a substantial ionic character.

As noted above, the graphene analog of monolayer black phosphorus, called phosphorene was isolated in 2014 by mechanical exfoliation [46]. However, in contrast to graphene which is gapless, phosphorene has a band gap. Due to its superior mechanical flexibility and electrostatic control, phosphorene is well suited for flexible nano-circuits. Subsequently, other similar monolayer materials were either proposed or synthesized that include silicene, germanene and stanene [69]. Notably, stanene is a two-dimensional topological insulator.

Time crystals: Recently, the concept of time crystals (both quantum and floquet) has gained significant attention [70]. In simple terms, crystals whose structure repeats in time can be called time crystals. Such crystals repeat in time because they are kicked periodically by laser pulsing or magnetic field, i.e. they are intrinsically out of equilibrium and break time translation symmetry. They are also called space-time crystals or four-dimensional crystals and are a novel type of *non-equilibrium matter*. In addition to being closely related to dynamical Casimir effect in the context of zero-point energy, they likely exhibit *topological order* which is potentially useful for quantum computing. Note that topological order violates the classical belief that ordering requires symmetry breaking. Time-dependent electromagnetic fields driving a crystalline material can tune its topological properties and may cause it to become a Floquet topological insulator. Thus the notion of a time crystal can be extended to Floquet time crystals [70].

1.5 Metrology and Techniques

1.5.1 High-Resolution Electron Microscopy

Measurements that can provide information about the underlying topological characteristics (e.g. genus, local connectivity) of a material through different experimental probes such as fluorescence, optical means, etc. constitute what we mean by topological metrology. In addition to Raman measurements, small angle X-ray (SAXS) and neutron scattering (SANS), scanning electron microscopy (SEM), transmission electron microscopy (TEM), stimulated Brillouin spectroscopy (SBS), various non-linear optical imaging techniques such as three-photon excitation fluorescence polarizing microscopy [71], X-ray tomography [72], electron holography and tomography [73] and Lorentz TEM [74] provide metrological means to study various aspects of materials topology.

1.5.2 Nonlinear Optical Imaging

In the context of liquid crystals and colloids many optical imaging techniques have been invoked to study topological defects such as Schlieren texture and even a more elaborate defect called a Hopf fibration [2]. In a uniaxial nematic crystal, the Schlieren defect is essentially the “director field”; it can be observed using a polarizing microscope. On the other hand, the Hopf fibration is an exotic texture which resembles a series of rings that are wrapped around a torus. It has been observed in chiral nematic liquid crystals with the aid of holographic optical tweezers in conjunction with fluorescence polarizing microscopy. Similarly, anisotropic optical absorption techniques have been invoked to study the electronic structure of many of the correlated topological materials including a giant, nonlinear optical response in Weyl semimetals [75].

1.5.3 X-Ray Tomography and Electron Holography

X-ray tomography is useful for characterizing porous media and porous networks including gyroid structures [76]. Similarly, for studying magnetic topological defects (e.g. vortices and skyrmions) and magnetic microstructures electron holography [73] and Lorentz TEM [74] are very useful techniques. Depending on the length scale of the magnetic nanostructure under consideration, magnetic force microscopy can be used as a complementary imaging technique.

1.5.4 X-Ray and Neutron Scattering

In order to link materials topology with metrology, small angle X-ray scattering (SAXS) and small angle neutron scattering (SANS) techniques can be used to reveal information about the structural and topological phases about nanoscale ordering in materials. Note that SAXS and SANS have been effectively used to study biomembranes, vesicles, certain supramolecular assemblies and di- and triblock copolymer morphologies in addition to understanding the structure of a variety of mesoporous materials such as zeolites and MOFs [2].

1.5.5 Elasticity and Deformation Energy Characterization

Biological vesicles and block copolymers having complex topologies with a genus up to $g = 3$ have been observed. In contrast, synthetic vesicles with very large values of g (~ 50) can occur [83]. To model these systems, we start with the Helfrich-Canham curvature (Fig. 1.10) free energy [84]: $E_s = \int dS [\frac{\kappa_b}{2}(H - H_0)^2 + \kappa_o K]$, where κ_b = bending rigidity, κ_o = Gaussian rigidity, dS = surface element. In addition, H_0 denotes spontaneous mean curvature, K and H are Gaussian and mean curvature, respectively. By using only topological means (e.g. Bogomol'nyi decomposition, which is usually invoked to study topological invariance and indicates that the Helfrich-Canham energy is greater than or equal to $4\pi\kappa_o$ times a genus dependent term), one can then calculate the elastic energy of deformation as a function of genus for vesicles [2], as shown in Fig. 1.11b. The energy increases proportionally with genus and eventually attains the value of 8π , consistent with a mathematical extrapolation called Wilmore conjecture. From topological analysis, one concludes that the spontaneous bending energy contribution from any deformation of the vesicles from their metastable shapes comprises two different topological sets: shapes of spherical topology ($g = 0$) and shapes of non-spherical topology ($g > 0$). One can readily apply these ideas to other topologies and materials. In a similar way, the deformation associated with negative curvature periodic minimal surfaces, e.g. double gyroids and Schwarzites, can be calculated, in particular under hydrostatic stress, if one assumes that only the lattice parameter changes under deformation. Analogously, graphene and carbon nanoribbons can exist in helicoidal shape. Their axial deformation can also be calculated by varying the pitch of the helicoid. In these cases, the elastic energy is proportional to the material's bulk (or axial) modulus and the Gaussian curvature.

Figure 1.11 shows the variation of Gaussian curvature K as a function of the surface parameter τ for three different values of the other surface parameter σ , and for the special direction when $\sigma = \tau$ [Through mathematical formalism for IPMS in the complex plane, the Gaussian curvature K can be explicitly expressed as a function of real variables τ and σ , [4, 5]. The expression for $K(\sigma, \tau)$ is invariant under the exchange of σ and τ and therefore, the two such figures must be identical [5]]. Note that for $\sigma = 0, 0.5$ and τ there is a minimum in K indicating elastically "soft" directions on the

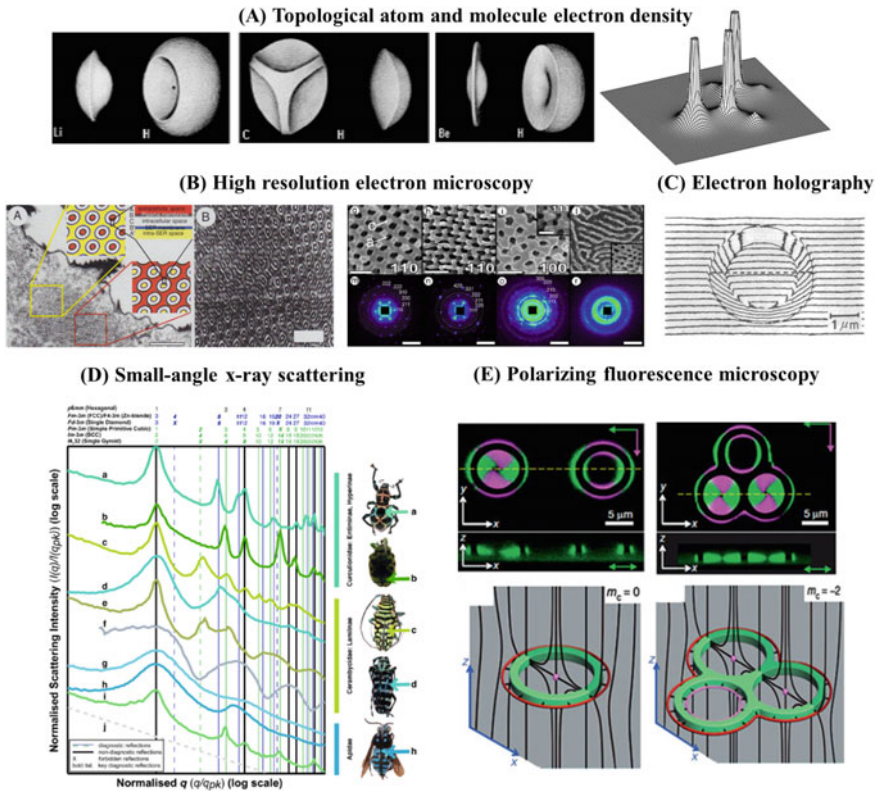


Fig. 1.10 Illustrations of various topological metrologies of **a** electron density distribution property of topological atoms and molecules [77, 78]. **b** Butterfly wing scale photonic nanostructure development using cross-section TEM depicting complex in-folding of the plasma membrane and SER membrane. The developing nanostructure shows the diagnostic motif of two concentric rings roughly in a triangular lattice. Yellow and red boxes highlight areas revealing different sections through the (110) plane of a polarized pentacontinuous core-shell double gyroid (color insets) [79]. Representative structural morphology of arthropod cuticular nanostructures and SAXS two-dimensional patterns from the photonic scales or setae [80], high-resolution electron microscopy revealing topological structures. **c** Interferogram of a toroidal ferromagnet measured using electron holography [81]. **d** Structural diagnoses of representative SAXS profiles of arthropod cuticular photonic nanostructures. **e** single- and triple handlebar ($g = 1, 3$, respectively) textures of colloidal particles that are non-spherical and dispersed in liquid crystals as obtained by three-photon excitation fluorescence polarizing microscopy (3PEF-PM) in addition to optical tweezers [82]

periodic minimal surface. However, for $\sigma = 1$ we observe a monotonically increasing “kink like” variation of K with τ . Also for the $\sigma = 0$ case, there are two values ($3\pi/50$ and $3\pi/5$) for which a local maximum is observed indicating elastically “hard” or stiff directions. Also note that the elastic energy density is directly proportional to K . Thus these curves provide a guide to the deformation energy behavior of Schwarzite surfaces.

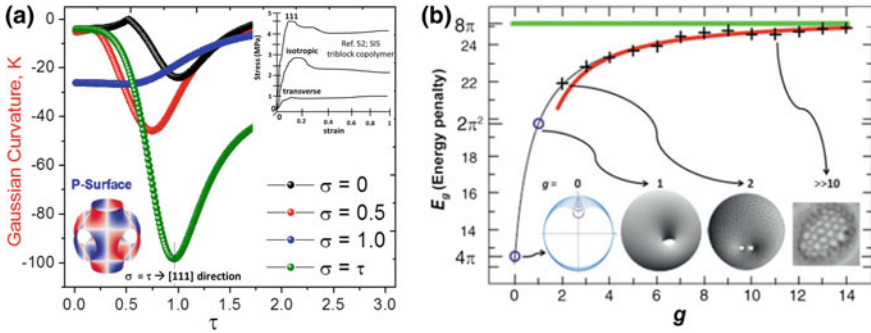


Fig. 1.11 **a** Variation of Gaussian curvature K for a minimal periodic surface such as Schwarzite as a function of τ for three different values of σ and for the special direction when $\sigma = \tau$ corresponding to various directions on the unit patch of the P-surface. The inset shows the stress-strain behavior in three different directions namely, $[111]$, isotropic and transverse directions for SIS triblock copolymer forming a double gyroid phase [85]. **b** Elastic deformation energy of vesicles (E_g) versus genus [86] where blue circles are exact values; crosses are numerical estimates computed with a (Brakke’s) surface evolver. Note that for large values of g the red curve is an estimated fit to the deformation energy. Finally, the green line is the asymptotic value of 8π

1.5.6 Topological Correlators and Other Metrics

Analogous to usual materials, the notions of two-point and higher order correlations can be generalized to topological correlations. The latter could conceivably be inferred from a combination of scattering techniques. Similarly, for nets and ramified structures one could envision obtaining network topology correlations (about local connectivity) from appropriately chosen momentum range in scattering experiments. Geometric measures such as curvature-curvature correlations (both in mean and Gaussian curvature) can complement the insights gained via topological correlations.

1.6 Computational Topology of Materials

Combining notions from topology and numerical algorithms, the field of computational topology has emerged. One of the key ideas in this context is the discovery of topology through algorithms. Although this topic belongs to the realm of computer science and mathematics, extending it to study the properties of topological materials opens a new avenue of investigation. This is of particular interest for materials involving network like structures, double gyroids, etc.

1.6.1 Topological Databases and Visualizing Topology

Over the past two decades topological databases and computer algorithms such as EPINET and TOPOS [87] have been developed. They are very useful in designing extended crystalline frameworks and architectures. In the context of Materials by Design, Directed Materials for Energy and Environment, and Materials Genome Initiative (MGI), it is now imperative to create databases for the properties of topological materials which can in turn be used to predict new topological materials with desired physical properties targeting specific applications (i.e. Topological Materials Informatics). On the other hand, the analysis of various databases using techniques from topology is called topological data analysis (TDA), and it is a growing area of research which can fruitfully be applied to study materials.

Many tools have been developed to visualize the topology of networks and that of vector fields (e.g. spin configuration, flow fields, etc.). Some examples include TOPO, Otter, TorusVis, Kiwi, RadialNet, among others. They also enable us to display various topological aspects of a structure such as genus and network node connectivity. Also, one can explore how local topology evolves or changes under parametric variation in a material. Adopting these tools to understand the structure and properties of topological materials can lead to an entirely new way of understanding materials we have discussed in this chapter.

1.6.2 Miscellaneous Topics

In this chapter, we have tried to cover a broad variety of topological materials and their properties. However, our exposure is not comprehensive as we have not addressed the fields of topological photonics, topological plasmonics (and metamaterials), mechanical metamaterials (or auxetic materials) as well as the use of topology in characterizing materials microstructure. For the sake of completeness we briefly mention these topics here.

Topological photonics: Inspired by the observation of topological phases in condensed matter (e.g. TI and TCI, see Fig. 1.12) and materials science, analogs of such phases have been realized in the photonic context ushering in the field of topological photonics [88]. An ingenious design of wave vector space topologies is enabling the creation of interfaces supporting entirely new states of light with many useful properties. For instance, one can create unidirectional waveguides in which light flows around large imperfections without back-reflection (akin to interfacial electron transport without dissipation in topological insulators in condensed matter [39, 40]). There has been significant progress in the realization of a whole slew of topological effects in photonic crystals, photonic quasicrystals, coupled resonators and metamaterials. In the near future one expects to discover topological mirrors and new applications of interacting photons by invoking nonlinearity and entanglement. Some of the technological advantages here involve decreased power consumption,

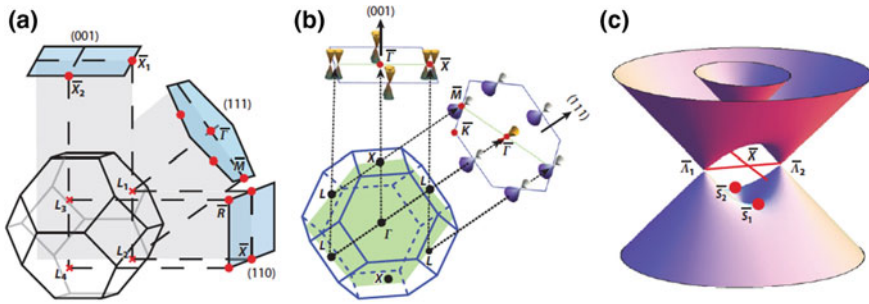


Fig. 1.12 Topological crystalline insulator. **a** High-symmetry points in the Brillouin zone and three projected surfaces for the rock-salt crystal structure. **b** Dirac cones in the (001) and (111) surface Brillouin zones. **c** Calculated dispersion for the (001) double Dirac cone surface state. Adapted from [42]

improved coherence in quantum links, avoiding use of isolators in photonic circuits, etc.

Topological plasmonics: Plasmonic excitations in Dirac materials including single and bilayer graphene and topological insulators are important both for a fundamental understanding of these materials as well as for their application in optoelectronic devices [89]. Recently an analogy between the usual two-dimensional magnetoplasmon [90] and p-wave topological superconductors has emerged. Analogs of photonic topology can be envisioned not only for surface plasmons but also for other bosonic systems such as magnons, phonons, excitons and exciton-polaritons. The key idea is that topological effects can be exploited to substantially improve the robustness of plasmonic, photonic and other devices in the presence of imperfections and various types of disorder.

Microstructure and topology: Statistical topology of cellular networks using Poisson-Voronoi cells has been recently developed along with a topological framework for local structure analysis and grain-growth microstructure characterization [91, 92]. Specifically, within a unified mathematical framework, local structure in both ordered and disordered materials can be classified by using the topology of the Voronoi cell associated with a particle (Fig. 1.13). For a given set of particles the Voronoi cell of a particle refers to a region in real space that is closer to the particle than to any other. This topological description of local structure offers many advantages for structural analysis compared to continuous descriptions. It also enables to identify which particles are associated with defects as opposed to belonging to specific (crystalline) phases. This versatile approach is also applicable to highly defected solids and glass-forming liquids. Moreover, through the distribution of different topological types the Voronoi topology aids the characterization of disordered systems in a statistical manner.

Another important concept that helps our understanding of microstructure is that of hyperuniformity [93]. One could think of unusual amorphous states of materials that lie between crystal and liquid as disordered many-particle hyperuniform sys-

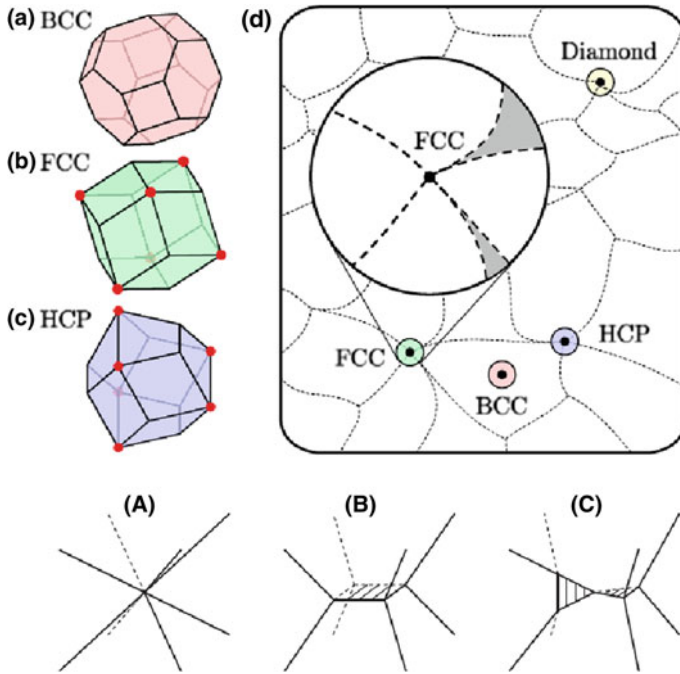


Fig. 1.13 Upper panel: **a**, **b** and **c** Voronoi cells of particles for the BCC, FCC and HCP crystals. Vertices where more than four Voronoi cells meet are indicated by red circles. Near these vertices small perturbations in particle positions lead to topological changes. **d** Space of all possible configurations of n neighbors; it can be divided into regions of constant Voronoi cell topology. Inset depicts the neighborhood around an FCC point. Lower panel: Sharing of an unstable vertex by six Voronoi cells in HCP or FCC crystals. A small perturbation can morph the vertex (in **A**) to either a four-sided face (in **B**) or a pair of contiguous triangular faces (in **C**). Adapted from [92]

tems. Put another way, in a hyperuniform system density fluctuations are completely suppressed at very large length scales, which means that the structure factor $S(\mathbf{k})$ tends to zero as the wave vector \mathbf{k} vanishes. It provides a unified framework to classify and categorize certain disordered configurations, crystals and quasicrystals. It is also important for understanding local fluctuations in the interfacial area of two-phase media.

1.7 Conclusion

Based on a series of eclectic examples, we elucidated that the topological concepts are beginning to take a firm foothold in materials science [2]. Our hope is that the emerging shift from a structure \rightarrow property \rightarrow functionality traditional paradigm to a new topology/geometry \rightarrow property \rightarrow functionality emerging paradigm will

assist materials scientists to study various usual and topological materials using the powerful interrelated concepts of (local) geometry and (global) topology. We illustrated this paradigm through a variety of materials including nanocarbon allotropes, soft matter, supramacromolecular assemblies, vesicles, biomembranes and MOFs.

An additional question is to understand the processing-structure-property (PSP) aspects of materials science for topological materials, i.e. how do synthesis and processing affect the topology of a material. In other words, how do we develop a processing-topology-property (PTP) based understanding of materials, which may lead to insights into interfaces between disparate topological materials and eventually to advanced manufacturing. This consideration naturally leads to another research frontier that is emerging: *topological dynamics*, i.e. keeping track of the time evolution of either the topology of or the relevant topological phase in a given material of interest.

The power and role of topology is turning out to be crucial in materials science in terms of unraveling certain types of defects (e.g. skyrmions, monopoles, hopfions, vortex lines) and in understanding an emerging class of topological materials with linear electronic dispersion such as Dirac materials and Weyl semimetals. Graphene, its two-dimensional siblings, e.g. silicene, germanene and phosphorene [46], in addition to topological insulators and topological superconductors are paving the way for unusual and technologically important properties. A variety of external perturbations including magnetic doping, electric and magnetic fields, light, disorder, temperature gradient, field gradients, strain and variation in film thickness can be used to alter and probe these fascinating materials. Inclusion of electronic correlations may lead to yet more exotic states of matter, e.g. fractional topological insulators [55].

We also discussed a variety of characterization techniques for topological materials ranging from optical imaging to electron holography, from fluorescence polarizing microscopy to Lorentz TEM, as well as small angle X-ray and neutron scattering. One aspect of this field that requires substantial progress and is now ripe for new ideas is that of topological metrology including use of topological correlations (both in real- and k-space) to characterize different material properties. The field of topological databases and informatics is still in its infancy. The importance of topology is thus ineluctable in materials science given the enormity of expected breakthroughs spanning fundamental and invaluable insights into modern and novel technologies.

Acknowledgements The authors acknowledge stimulating and helpful discussions with several colleagues around the world over the past decade. This work was supported in parts by the U.S. Department of Energy and Western Kentucky University Research Foundation Inc.

References

1. S. Gupta, A. Saxena, MRS Bull. News Feature, Oct. 18 (2016); F. Ghahari, D. Walkup, C. Gutiérrez, J.F.R.- Nieva, Y. Zhao, J. Wyrick, F.D. Natterer, W.G. Cullen, K. Watanabe, T. Taniguchi, L.S. Leitov, N.B. Zhitenev, J.A. Stroscio, Science **356**, 845 (2017)
2. S. Gupta, A. Saxena, MRS Bull. **39**, 265 (2014)

3. S. Gupta, A. Saxena, J. Raman Spectrosc. **40**, 1127 (2009)
4. S. Gupta, A. Saxena, J. Appl. Phys. **109**, 074316 (2011)
5. S. Gupta, A. Saxena, J. Appl. Phys. **112**, 114316 (2012)
6. V. Meunier, Ph Lambin, A.A. Lucas, Phys. Rev. B **57**, 14886 (1998)
7. J.C. Charlier, G.M. Rignanese, Phys. Rev. Lett. **86**, 5970 (2001)
8. M.W. Iqbal, A.K. Singh, M.Z. Iqbal, J. Eom, J. Phys.: Condens. Matter **24**, 335301 (2012)
9. V. Mennella, G. Monaco, L. Colangeli, E. Bussoletti, Carbon **33**, 115 (1995)
10. G. Toulouse, M. Kléman, J. Phys. Lett. **37**, L149 (1976)
11. G. E. Volovik, V. P. Mineyev, Zh. Eksp. Teor. Fiz. Pis'ma Red. **24**, 605 (1976)
12. J. Wright, N.D. Mermin, Rev. Mod. Phys. **61**, 385 (1989)
13. X. Xing, J. Stat. Phys. **134**, 487 (2009)
14. B. Senyuk, Q. Liu, S. He, R.D. Kamien, R.B. Kusner, T.C. Lubensky, I.I. Smylukhov, Nature **493**, 200 (2013)
15. B.G. Chen, P.J. Ackerman, G.P. Alexander, R.D. Kamien, I.I. Smylukhov, Phys. Rev. Lett. **110**, 237801 (2013)
16. G.S. Settles, *Schlieren and Shadowgraph Techniques: Visualizing Phenomena in Transparent Media* (Springer, Berlin, 2001)
17. A.T. Skjeltorp, *Knots and Applications to Biology, Chemistry and Physics* (Springer, NY, 1996)
18. S.R. Batten, N.R. Champness, X.-M. Chen, J.G.-Martinez, S. Kitagawa, S.L. Öhrström, M. O'Keefe, M.P. Suh, J. Reedijk, Pure Appl. Chem. **85**, 1715 (2013)
19. A.K. Cheetham, G. Férey, T. Loiseau, Angew. Chem. Inter. Ed. **38**, 3268 (1999)
20. J. Cejka (ed.), *Metal-Organic Frameworks Applications from Catalysis to Gas Storage* (Wiley-VCH, 2011)
21. S.T. Hyde, G.E. Schröder-Turk, Interface Focus **2**, 529 (2012)
22. T. Ishøy, K. Mortensen, Langmuir **21**, 1766 (2005)
23. N. Hadjichristidis, S. Pispas, G. Floudas, *Block Copolymers: Synthetic Strategies, Physical Properties and Applications* (Wiley, NY, 2003)
24. E. Sezgin, H.-J. Kaiser, T. Baumgart, P. Schwille, K. Simons, I. Levental, Nat. Protoc. **7**, 1042 (2012)
25. D. Zhao, D.J. Timmons, D. Yuan, H.-C. Zhou, Acc. Chem. Res. **44**, 123 (2011)
26. J. Katsaras, T. Gutberlet (eds.), *Lipid Bilayers—Structure and Interactions* (Springer, Berlin-Heidelberg, 2001)
27. H.L. Leertouwer, B.D. Wilts, D.G. Stavenga, Opt. Exp. **19**, 24061 (2011)
28. B.D. Wilts, K. Michielsen, J. Kuipers, H. De Raedt, D.G. Stavenga, Proc. R Soc. B **279**, 2524 (2012)
29. B. Yan, S.-C. Zhang, Rep. Prog. Phys. **75**, 096501 (2012)
30. X.-L. Qi, T.L. Hughes, S.-C. Zhang, Phys. Rev. B **78**, 195424 (2008)
31. A. Roy, D.P. DiVincenzo, *Topological Quantum Computing*, [arXiv:1701.05052](https://arxiv.org/abs/1701.05052)
32. S. Tanda, T. Tsuneta, Y. Okajima, K. Inagaki, K. Yamaya, N. Hatakenaka, Nature **417**, 397 (2002)
33. T. Tsuneta, S. Tanda, J. Cryst. Growth **267**, 223 (2004)
34. T. Matsuura, M. Yamanaka, N. Hatakenaka, T. Matsuyama, S. Tanda, J. Cryst. Growth **297**, 157 (2006)
35. R.E. Goldstein, H.K. Moffatt, A.I. Pesci, R.L. Ricca, Proc. Natl. Acad. Sci. (USA) **107**, 21979 (2010)
36. D.M. Kleiman, D.F. Hinz, Y. Takato, E. Fried, Soft Matter **12**, 3750 (2016)
37. T.O. Wehling, A.M. Black-Schaffer, A.V. Balatsky, Adv. Phys. **63**, 1 (2014)
38. J. Cayssol, Comp. Rend. Physique **14**, 760 (2013)
39. M.Z. Hassan, C.L. Kane, Rev. Mod. Phys. **82**, 3045 (2010)
40. X.L. Qi, S.-C. Zhang, Rev. Mod. Phys. **83**, 1057 (2011)
41. L. Fu, Phys. Rev. Lett. **106**, 106802 (2011)
42. Y. Ando, L. Fu, Annu. Rev. Condens. Matter Phys. **6**, 361 (2015)
43. B. Aufray, A. Kara, S.B. Vizzini, H. Oughaddou, C. LeAndri, G. Le Lay, Appl. Phys. Lett. **96**, 183102 (2010)

44. M.E. Davila, L. Xian, S. Cahangirov, A. Rubio, G. Le Lay, *New J. Phys.* **16**, 095002 (2014)
45. B.G. Kim, H.J. Choi, *Phys. Rev. B* **86**, 115435 (2012)
46. H. Liu, A.T. Neal, Z. Zhu, Z. Luo, X. Xu, D. Tomanek, P.D. Ye, *ACS Nano* **8**, 4033 (2014)
47. Y. Xu, B. Yan, H.-J. Zhang, J. Wang, G. Xu, P. Tang, W. Duan, S.-C. Zhang, *Phys. Rev. Lett.* **111**, 136804 (2013)
48. G. Bian et al., *Nat. Commun.* **7**, 10556 (2016)
49. S.-Y. Xu et al., *Science* **349**, 613 (2015)
50. B.Q. Lv et al., *Phys. Rev. X* **5**, 031013 (2015)
51. V. Mourik, K. Zuo, S.M. Frolov, S.R. Plissard, E.P.A.M. Bakkers, L.P. Kouwenhoven, *Science* **336**, 1003 (2012)
52. S. Sasaki, M. Kreiner, K. Segawa, K. Yada, Y. Tanaka, M. Sato, Y. Ando, *Phys. Rev. Lett.* **107**, 217001 (2011); M. Sato, Y. Ando, *Rep. Prog. Phys.* **80**, 076501 (2017)
53. V.S. Pribiag, A.J.A. Beukman, F. Qu, M.C. Cassidy, C. Charpentier, W. Wegscheider, L.P. Kouwenhoven, *Nat. Nanotechnol.* **10**, 593 (2015)
54. D.-T. Tran, A. Dauphin, N. Goldman, P. Gaspard, *Phys. Rev. B* **91**, 085125 (2015)
55. M. Levin, A. Stern, *Phys. Rev. Lett.* **103**, 196803 (2009)
56. O. Vafek, A. Vishwanath, *Ann. Rev. Cond. Mat. Phys.* **5**, 83 (2014)
57. X. Wan, A.M. Turner, A. Vishwanath, S.Y. Savrasov, *Phys. Rev. B* **83**, 205101 (2011)
58. A.A. Burkov, L. Balents, *Phys. Rev. Lett.* **107**, 127205 (2011)
59. B. Yan, C. Felser, *Ann. Rev. Cond. Mat. Phys.* **8**, 337 (2017)
60. S. Jia, S.-Y. Xu, M.Z. Hasan, *Nat. Mater.* **15**, 1140 (2016)
61. S. Zhang, I. Gilbert, C. Nisoli, G.-W. Chern, M.J. Erickson, L. O'Brien, C. Leighton, P.E. Lammert, V.H. Crespi, P. Schiffer, *Nature* **500**, 553 (2013)
62. P. Milde, D. Kohler, J. Seidel, L.M. Eng, A. Bauer, A. Chacon, J. Kindervater, S. Muhlbauer, C. Pfleiderer, S. Buhrandt, C. Schutte, A. Rosch, *Science* **340**, 1076 (2013)
63. S.H. Zhang, J. Zhou, Q. Wang, X.S. Chen, Y. Kawazoe, P. Jena, *Proc. Natl. Acad. Sci. (USA)* **112**, 2372 (2015)
64. S. Zhang, Q. Wang, Y. Kawazoe, P. Jena, *J. Am. Chem. Soc.* **135**, 18216 (2013)
65. A. Lopez-Bezanilla, I. Martin, P.B. Littlewood, *Sci. Rep.* **6**, 33220 (2016)
66. A. Lopez-Bezanilla, *J. Phys. Chem. C* **120**, 17101 (2016)
67. J. Zhang, H.J. Liu, L. Cheng, J. Wei, J.H. Liang, D.D. Fan, J. Shi, X.F. Tang, Q.J. Zhang, *Sci. Rep.* **4**, 6542 (2014)
68. Z. Wang, X.-F. Zhou, X. Zhang, Q. Zhu, H. Dong, M. Zhao, A.R. Oganov, *Nano Lett.* **15**, 6182 (2015)
69. C.-C. Liu, H. Jiang, Y. Yao, *Phys. Rev. B* **84**, 195430 (2011)
70. D.V. Else, B. Bauer, C. Nayak, *Phys. Rev. Lett.* **117**, 090402 (2016)
71. B.G. Chen, P.J. Ackerman, G.P. Alexander, R.D. Kamien, I.I. Smalyukh, *Phys. Rev. Lett.* **110**, 237801 (2013)
72. L. Salvo, M. Suery, A. Marmottant, N. Limodin, D. Bernard, *Comput. Rend. Phys.* **11**, 641 (2010)
73. P.A. Midgley, R.E. Dunin-Borkowski, *Nat. Mater.* **8**, 271 (2009)
74. A.K. Petford-Long, M. De Graef, *Lorentz Microscopy, Characterization of Materials*, 1–15 (Wiley Online Library, 2012)
75. L. Wu, S. Patankar, T. Morimoto, N.L. Nair, E. Thewalt, A. Little, J.G. Analytis, J.E. Moore, J. Orenstein, *Nat. Phys.* **13**, 350 (2017)
76. H.K. Chae, D.Y. Siberio-Perez, J. Kim, Y.-B. Go, M. Eddaoudi, A.J. Matzger, M. O'Keefe, O.M. Yaghi, *Nature* **427**, 523 (2004)
77. R.F.W. Bader, C. Matta, *J. Phys. Chem. A* **108**, 8385 (2004)
78. R.F.W. Bader, D.E. Fang, *J. Chem. Theory Comput.* **1**, 403 (2005)
79. V. Saranathan, C.O. Osujib, S.G.J. Mochrie, H. Nohb, S. Narayanan, A. Sandy, E.R. Dufresne, R.O. Pruma, *Proc. Natl. Acad. Sci. (USA)* **107**, 11676 (2010)
80. V. Saranathan, A.E. Seago, A. Sandy, S. Narayanan, S.G.J. Mochrie, E.R. Dufresne, H. Cao, C.O. Osuji, R.O. Prumand, *Nano Lett.* **15**, 3735 (2015)

81. A. Tonomura, H. Umezaki, T. Matsuda, N. Osakabe, J. Endo, Y. Sugita, *Phys. Rev. Lett.* **51**, 331 (1983)
82. B. Senyuk et al., *Nature* **493**, 200 (2013)
83. X. Michalet, D. Bensimon, *Science* **269**, 666 (1995)
84. R. Lipowsky, *Encyclopedia of Applied Physics* **23**, 199 (1998)
85. B.J. Dair, A. Avgeropoulos, N. Hadjichristidis, E.L. Thomas, *J. Mater. Sci.* **35**, 5207 (2000)
86. J. Benoit, A. Saxena, T. Lookman, *J. Phys. A* **34**, 9417 (2001)
87. <http://www.topos.samsu.ru> and <http://www.epinet.anu.edu.au/reference>
88. L. Liu, J.D. Joannopoulos, M. Soljacic, *Nat. Photonics* **8**, 821 (2014)
89. T. Stauber, *J. Phys.: Condens. Mater* **26**, 123201 (2014)
90. D. Jin et al., *Nat. Commun.* **7**, 13486 (2016)
91. E.A. Lazar, J.K. Mason, R.D. MacPherson, D.J. Srolovitz, *Phys. Rev. Lett.* **109**, 095505 (2012)
92. E.A. Lazar, J. Han, D.J. Srolovitz, *Proc. Natl. Acad. Sci. (USA)* **112**, E5769 (2015)
93. S. Torquato, *Phys. Rev. E* **94**, 022122 (2016)